**ARTICLE** OPEN

Check for updates

# Sub-picosecond photo-induced displacive phase transition in two-dimensional MoTe$_2$

Bo Peng [1,2,3], Hao Zhang [1✉], Weiwen Chen[1], Bowen Hou [1], Zhi-Jun Qiu[4], Hezhu Shao[5], Heyuan Zhu [1✉], Bartomeu Monserrat[3,6], Desheng Fu [7✉], Hongming Weng [2] and Costas M. Soukoulis[8]

Photo-induced phase transitions (PIPTs) provide an ultrafast, energy-efficient way for precisely manipulating the topological properties of transition-metal ditellurides and can be used to stabilize a topological phase in an otherwise semiconducting material. Using first-principles calculations, we demonstrate that the PIPT in monolayer MoTe$_2$ from the semiconducting 2H phase to the topological 1T′ phase can be triggered purely by electronic excitations that soften multiple lattice vibrational modes. These softenings, driven by a Peierls-like mechanism within the conduction bands, lead to structural symmetry breaking within sub-picosecond timescales, which is shorter than the timescale of a thermally driven phase transition. The transition is predicted to be triggered by photons with energies over 1.96 eV, with an associated excited carrier density of $3.4 \times 10^{14}$ cm$^{-2}$, which enables a controllable phase transformation by varying the laser wavelength. Our results provide insight into the underlying physics of the phase transition in 2D transition-metal ditellurides and show an ultrafast phase-transition mechanism for manipulation of the topological properties of 2D systems.

## INTRODUCTION

A photo-induced phase transition (PIPT), resulting from cooperative electron–lattice interactions through transiently changing the electronic states of the solid by photoexcitations[1], is completely different from thermally or pressure-induced phase transitions. A PIPT not only gives access to different phases in the solid to explore anomalous properties absent in the ground-state phase[2] but also enables precisely controllable phase transitions towards target structures with desired physical properties at high speeds[3]. Thus, the initial discovery of a PIPT in organic charge transfer crystals has triggered great interest in a variety of fields[4]. Compared with the vast number of materials exhibiting thermodynamic phase transitions, there are still very few solids undergoing a PIPT, and many investigations currently focus on bulk crystals possessing one-dimensional (1D) correlated electron chains in which PIPTs may be easily triggered due to inherent instabilities caused by electron–electron and electron–lattice interactions in these quasi-1D systems[1,5].

As an emerging platform for PIPTs, two-dimensional (2D) and layered transition-metal ditellurides exhibit polymorphisms with distinct physical properties[6–8]. Recent experimental evidence for a PIPT in MoTe$_2$ and WTe$_2$ shows that structural phase transitions often involve abrupt changes in the electronic structure such as the emergence of novel topological states[9–11]. For instance, in few-layer MoTe$_2$, an irreversible transition from a semiconducting hexagonal 2H phase to a topological distorted octahedral 1T′ phase occurs under laser irradiation, which can be used to fabricate an ohmic heterophase homojunction with accurate

control of micrometer-patterning in a desired area[9]. The phase transition is irreversible, because the 1T′ phase formed in the electronically excited state is metastable, and to return to the ground-state 2H phase, the system has to overcome a potential barrier of around 0.71 eV[12,13]. The laser-induced 1T′ MoTe$_2$ is stable for more than 1 week in ambient conditions without any protection[14]. Moreover, the structural distortion from the 2H to the 1T′ phase results in an intrinsic band inversion between Te $p$ and Mo $d$ bands[15,16], enabling ultrafast manipulation of the topological character of MoTe$_2$. The topological phase also displays gate-tunable superconductivity, providing a new potential platform to realize Majorana bound modes[17,18].

Despite all this progress, the microscopic nature of the PIPT remains unclear. Triggered by external stimulation by light, the system undergoes changes in temperature, strain, electronic excitation, chemical state, and lattice vibrational modes. The transition may depend on one of these factors or on a combination of them[9,19]. One proposal is that Te vacancies created by irradiation trigger the local phase transition[9,20,21]. Other theoretical and experimental studies have argued that accumulated heat is a main driving force for the phase transition[14,20]. Moreover, a strain-induced phase transition has been observed in monolayer MoTe$_2$[22,23]; thus, laser-induced thermal strain may also contribute to the observed phase transition. Yet, another explanation is that it is the electronic excitation that plays a critical role in the phase transition[12,13]. Overall, the transition mechanism is still debated.

In this work, we demonstrate that the phase transition of monolayer MoTe$_2$ can be triggered by photoexcitation of carriers

[1]Key Laboratory of Micro and Nano Photonic Structures (MOE), Department of Optical Science and Engineering, Fudan University, Shanghai 200433, China. [2]Beijing National Laboratory for Condensed Matter Physics and Institute of Physics, Chinese Academy of Sciences, Beijing 100190, China. [3]Cavendish Laboratory, University of Cambridge, J. J. Thomson Avenue, Cambridge CB3 0HE, UK. [4]State Key Laboratory of ASIC and System, School of Information Science and Technology, Fudan University, Shanghai 200433, China. [5]Wenzhou Key Laboratory of Micro-nano Optoelectronic Devices, College of Electrical and Electronic Engineering, Wenzhou University, Wenzhou 325035, China. [6]Department of Materials Science and Metallurgy, University of Cambridge, 27 Charles Babbage Road, Cambridge CB3 0FS, UK. [7]Faculty of Engineering, Department of Electronics and Materials Sciences and Department of Optoelectronics and Nanostructure Science, Graduate School of Science and Technology, Shizuoka University, Hamamatsu 432-8561, Japan. [8]Department of Physics and Astronomy and Ames Laboratory, Iowa State University, Ames, Iowa 50011, USA. ✉email: zhangh@fudan.edu.cn; hyzhu@fudan.edu.cn; fu.tokusho@shizuoka.ac.jp
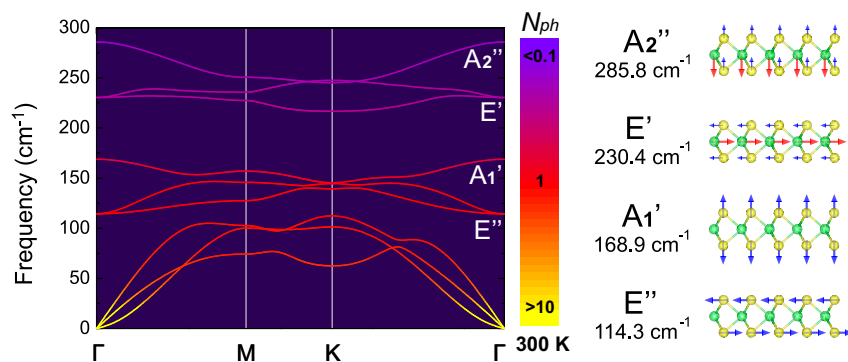
**Fig. 1 Lattice dynamics in the ground states.** Phonon dispersion of 2H MoTe$_2$ monolayer and vibrational modes for optical phonons at the $\Gamma$ point. The phonon occupation number is determined from the Bose–Einstein distribution function at 300 K.

alone. Using first-principles calculations, we study the excited-state properties of 2H MoTe$_2$ at photoexcitation energies $E$ of 1.58 eV (785 nm), 1.96 eV (633 m), 2.34 eV (532 nm), 2.42 eV (514 nm), and 2.63 eV (473 nm) by exciting all available electrons consistent with these energies. We find that a soft-mode displacive phase transition occurs for $E > 1.96$ eV. Photoexcitation modifies the electronic potential, resulting in a complete softening of the lattice vibrations that leads to spontaneous structural distortions with new equilibrium positions for the atoms. This structural transition takes place within one picosecond, shorter than the timescale for the photoexcited electrons to transfer their energy to the lattice. We also rule out a thermally driven or a strain-induced phase transition under laser irradiation by comparing the thermodynamic stability of 2H and 1T' MoTe$_2$ monolayers. Our findings not only reveal the potential origin of the PIPT in 2D transition-metal ditellurides but also provide new insight into the observed dynamic transitions in their three-dimensional (3D) counterparts, another question that remains unclear[10,24,25].

## RESULTS AND DISCUSSION

### Lattice mode softening

We start by examining atomic displacements in the excited state to see whether (and how) a phase transition may be triggered. With $D_{3h}$ point group, the irreducible representations of the vibrational modes in the 2H phase at the $\Gamma$ point are expressed as[26]

$$\Gamma_{2H} = E'' + A_1' + E' + A_2''. \tag{1}$$

The calculated phonon dispersion is shown in Fig. 1 and the calculated lattice mode frequencies are consistent with previous reports[27,28].

The three modes E'', E', and A$_2''$ correspond to the three primary lattice distortions along the pathway from the 2H to the 1T' phase, so could play a role in triggering the phase transition (for the three primary lattice distortions, see "Crystal Structures" in Supplementary Information). We calculate the potential energy as a function of displacement amplitude of these vibrations under different photoexcitation energies and corresponding carrier densities to investigate potential structural instabilities. The results are summarized in Fig. 2a-c, with the energy of the excited 1T' phase set to zero for comparing the relative stability between the 2H and 1T' phases. In the ground state, the energy of the 2H phase is 80 meV lower than that of the 1T' phase. However, as the system is optically excited, the 2H phase becomes energetically less favorable than the 1T' phase due to population inversion[12,13].

For the E'' mode (corresponding to the opposite in-plane motion of top and bottom Te layers), the Te atoms vibrate harmonically around their equilibrium positions before photo-excitation. With increasing excitation energy (and corresponding excited carrier density), the potential energy surface gradually

flattens, and a double-well potential forms at $E > 1.96$ eV. Thus, a distorted octahedral structure can form as atoms move to new equilibrium positions (Fig. 2d). A similar situation occurs for the A$_2''$ mode (an out-of-plane displacement of Mo atoms and an opposite-direction displacement of Te atoms). For $E > 1.96$ eV, the Mo atoms can bounce up or down to the two minimum energy sites of the new double-well potential, whereas the Te atoms move in opposite directions, leading to an out-of-plane distorted variant of 2H MoTe$_2$ (Fig. 2f). The evolution of the E' mode under irradiation is slightly different. This mode is composed of in-plane displacements with the single Mo layer and the two Te layers moving opposite to each other. Increasing $E$ lowers the energy barrier for positive displacements along the eigenvector of the E' mode. The barrier becomes a deep well at 2.63 eV, leading to the atomic distortion shown in Fig. 2e, with distorted in-plane atomic positions yielding a twisted octahedral coordination around Mo atoms. It should be noted that at 2.63 eV this mode dominates, but at lower energies the potential along the E' mode still exhibits a barrier, whereas both E'' and A$_2''$ modes show double-well potential energy surfaces, and therefore the latter two dominate in that regime. All three distortions of the corresponding mode eigenvectors are along the phase transition pathway from 2H to 1T' MoTe$_2$. The full transition from 2H to 1T' MoTe$_2$ probably occurs along a higher-dimensional path in configuration space in which photoexcitation lowers the energy barrier from 0.77 eV to 0.08 eV[13], but our results suggest that the softening of these key modes can initiate the PIPT with a purely electronic mechanism.

### Critical excitation energy $E_C$

The transition from a single-well potential to a double-well potential shown in Fig. 2a–c indicates a displacive phase transition, which involves a phonon frequency that falls to zero at a critical excitation energy $E_C$ and corresponding excited carrier density. These zero-frequency soft modes drive the crystal instability along the displacements of the corresponding mode eigenvectors, leading to spontaneous symmetry breaking[29,30]. We examine the soft-mode behavior under optical excitation in the framework of Landau theory for the E'' and A$_2''$ modes that soften at lower energies. For a soft-mode displacive phase transition, the order parameter can be chosen as the amplitude of the distortion of the soft-mode eigenvector $u$[29]. The lattice potential energy, equivalent to the free energy in the Landau theory[31,32], can be expressed by a fourth order even polynomial expansion of the order parameter $u$

$$V(u) = a + \frac{b}{2}u^2 + \frac{c}{4}u^4, \tag{2}$$

where the harmonic prefactor $b$ is equal to the square of the soft-mode phonon frequency $\omega^2$[29,33]. Before the phase transition, there

**(a)** E''    **(b)** E'    **(c)** A₂''

0 eV
1.58 eV
1.96 eV
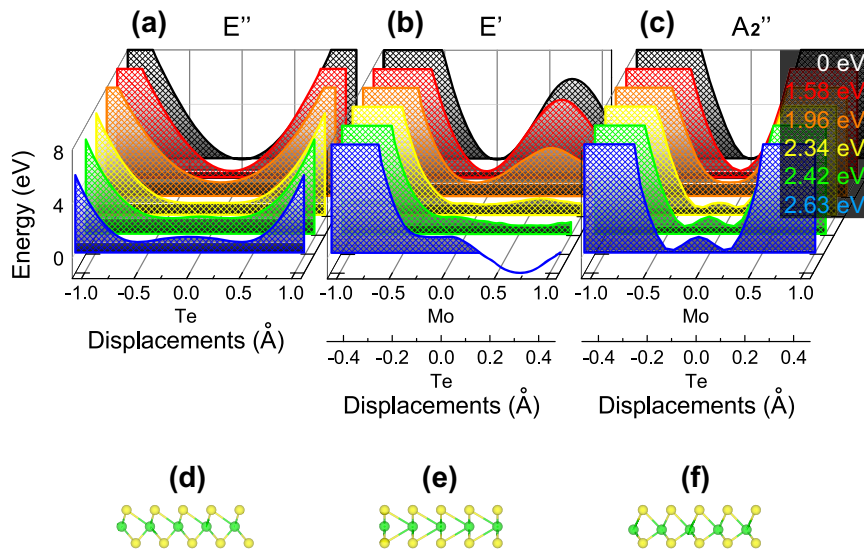2.34 eV
2.42 eV
2.63 eV

**(d)**    **(e)**    **(f)**

**Fig. 2 Lattice dynamics in the excited states.** Potential energy surface at different excitation energies along the eigenvectors of (**a**) E'', (**b**) E', and (**c**) $A_2''$ modes, and their corresponding structures (**d**–**f**) at the minima of the potential energy surface at 2.63 V.
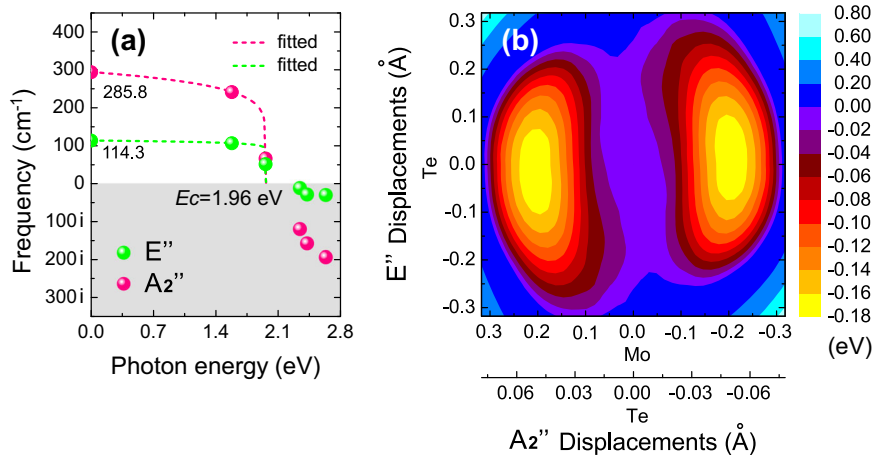
**Fig. 3 Analysis of the E'' and $A_2''$ modes. a** Phonon frequency of the E'' and $A_2''$ modes as a function of laser excitation energy. **b** Energy surface in the plane spanned by the two soft modes. Each contour line represents an energy increase of 0.02 eV.

is a single-well potential, corresponding to $b > 0$ ($c$ is a small positive value with a much weaker $E$ dependence). When $b$ becomes negative, $V(u)$ becomes a double-well function with minima at $u = \pm\sqrt{-b/c}$ and a local maximum value at $u = 0$. Therefore, the phonon softening can be described quantitatively by calculating the phonon frequencies of the two symmetric E'' and $A_2''$ modes as a function of photoexcitation energy. As shown in Fig. 3a, at 1.58 eV both modes soften slightly and drop significantly at 1.96 eV. The phonon frequency becomes imaginary for $E > 1.96$ eV, confirming again that a soft-mode phase transition occurs at $E > 1.96$ eV. It should be noted that at $E_C = 1.96$ eV, the potential energy surface of the E' mode is still a single well. The energy surface in the subspace spanned by both soft modes is calculated to further evaluate the spontaneous lattice distortions. Figure 3b shows the energy surface mapped on the plane spanned by the two soft modes E'' and $A_2''$ at the photoexcitation energy of 2.34 eV. These results suggest that the $A_2''$ mode dominates the distortion; thus, the PIPT is probably triggered along that distortion.

In the Landau theory, the phase transition occurs at $b = 0$. For temperature-driven ferroelectric/magnetic phase transitions, $b \propto (T - T_0)$, giving the well-known Curie–Weiss law[31]. In the detailed

analysis of the potential well of the $A_2''$ mode, we find $b \propto (E_C - E)^\gamma$, where $E_C = 1.96$ eV and $\gamma = 0.24$. As $b = \omega^2$, we fit the mode frequencies as a function of $E$ by $\omega \propto (E_C - E)^{\gamma/2}$, as shown in Fig. 3a. The obtained $E_C = 1.96$ eV is in good agreement with the change of electron distribution (Fig. 4b), from which one can see that the electron localization function also changes completely by $E \geq 1.96$ eV. A similar $E_C$ is also predicted for the E'' mode in Fig. 3a. Thus, our results suggest that the lattice distortions occur spontaneously after photoexcitation. Our prediction of photo-induced lattice mode softenings, marked by clear changes in both Raman and infrared spectra (E'' is Raman active and $A_2''$ is infrared active), can be verified experimentally by ultrafast coherent phonon spectroscopy[24] or second harmonic generation[34].

For a thermally induced phase transition, $b = \tilde{b}(T - T_0)$, where $\tilde{b}$ is a positive constant[29], the potential well changes gradually with temperature towards the phase transition. In contrast, in a PIPT, the potential well change is determined by the number of excited carriers, which is related to the excitation energy $E$ and the density of states (DOS). For instance, when $E$ is only slightly larger than the band gap, few electrons are excited to the conduction bands, leading to a negligible change of the potential well. Thus,
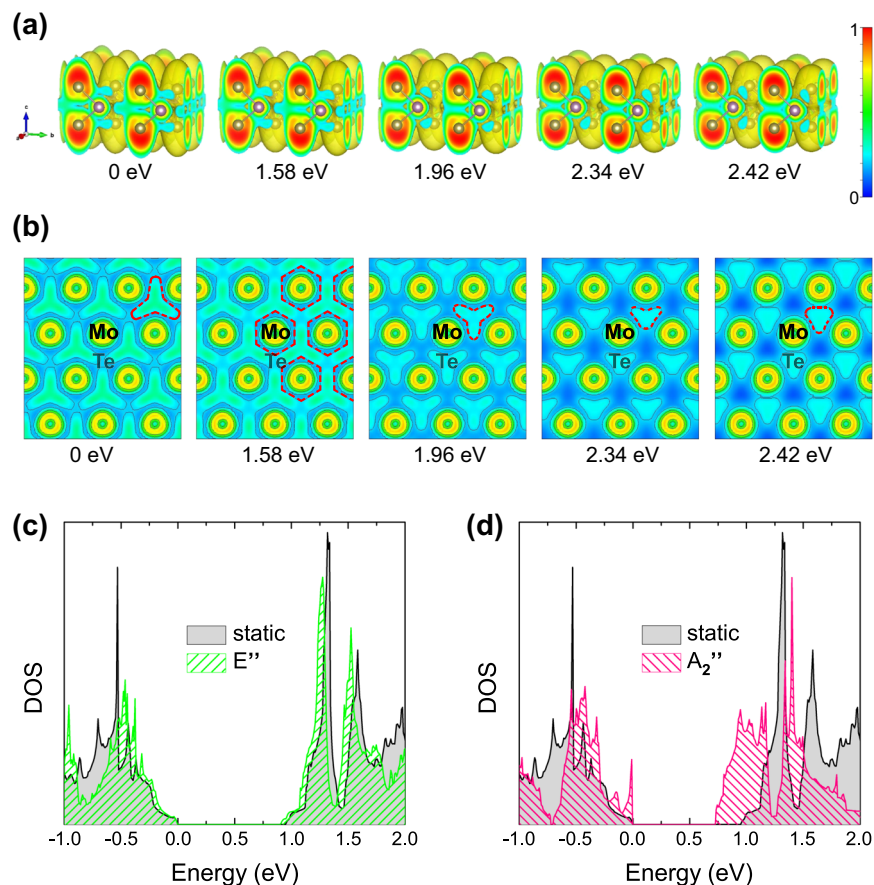
**Fig. 4  Microscopic mechanism for PIPT. a** 3D and **b** top view (Mo layer) of the electron localization function of 2H MoTe$_2$ at different excitation energies. The electron localization function from 0 to 1 is shown by colors from navy to red. The isosurface for the electron localization function in **a** is 0.2. Static lattice DOS (gray) compared with the DOS along the eigenvector of the (**c**) E'' (green) and (**d**) A$_2''$ (pink) phonon modes, with the displacement amplitudes corresponding to the potential minimum at 2.34 eV.

in the PIPT, $b$ has a much weaker $E$ dependence than the $T$ dependence in a thermally induced phase transition, leading to a much smaller $\gamma$.

**Photo-induced changes in the electronic state**

We next investigate the electronic state to rationalize the phonon softening upon photoexcitation discussed above. When a solid undergoes a structural phase transition, the ionic positions change because the symmetry of the electronic potential changes[35]. Light-induced electronic excitations in the 2H lattice may be responsible for such a change in the electronic potential. Figure 4a shows the 3D electron localization function of 2H MoTe$_2$ at different photoexcitation energies. As shown in Fig. 4b, the electron distribution around Mo atoms changes from isolated triangles (dashed red line) at 0 eV to connected hexagons (dashed red line) at 1.58 eV. As the excitation energy increases further to 1.96 eV, the electrons in the Mo layer gather between top and bottom Te atoms, and the in-plane triangles around Mo atoms appear once again, but with a reversed orientation compared with the ground state, indicating an electronic potential change. As the excitation energy increases to 2.34 eV, the inverted-triangle region of the electron density shrinks.

Figure 4c, d show a comparison of the DOS calculated for the static lattice and for the lattice distorted along the E'' and A$_2''$ phonon modes, with the displacement amplitudes corresponding to the potential minimum at 2.34 eV. As expected from the discussion in Figs. 2 and 3, the A$_2''$ mode distortion leads to a larger change in the DOS: there is a significant redistribution of DOSs in

the conduction band towards lower energies. A similar picture emerges for the E'' mode, but in that case the changes are small. In the ground state the conduction band is empty and therefore a redistribution of the DOSs towards lower energies does not affect the total energy of the system. However, upon photoexcitation, the conduction bands become occupied and it then becomes energetically favorable to undergo a lattice distortion to red shift the conduction bands and lower the overall energy of the system. This is analogous to the Peierls mechanism and provides a microscopic picture for the driving force behind the mode softening induced by photoexcitation. We note that the DOS around the valence band maximum also changes, and when those states are occupied in the ground state, the distortion leads to an energy increase as expected. However, under photoexcitation those states are unoccupied (holes), and the DOS redistribution has a minor effect on the total energy.

**Excited carrier concentrations**

As discussed above, for a given photoexcitation energy we consider that the number of incoming photons is as large as necessary to excite all available electrons that can be excited at the given laser energy. Therefore, the excited carrier concentration becomes a function of the excitation energy. Table 1 shows the excited carrier concentrations $n$ under different excitation energies. The excited carrier density at 1.96 eV is $3.4 \times 10^{14}$ cm$^{-2}$, corresponding to an excited carrier density of 2.9%. We also estimate the maximum amount of electron-hole pairs generated by a femtosecond laser with a fluence of 100 mJ/cm$^2$ assuming

that no saturation occurs (for the calculations of the maximum amount of electron-hole pairs, see "Within 20 fs of Laser Excitation" in Supplementary Information). At 1.96 eV, excitation of up to 10.2% is possible for a laser pulse with a fluence of 100 mJ/cm$^2$ (see Table 1) and thus the excited carrier concentrations in our calculations are experimentally accessible. As a PIPT can take place for excitations over 2.9%, a laser pulse with a minimum fluence of 28 mJ/cm$^2$ is needed to induce a phase transition at 1.96 eV. This is consistent with the experimental fact that with insufficient laser fluence, the phase transformation cannot take place even for long irradiation times[9,14].

The excited carrier population is related to the DOS[36]. Optical transitions are dominated by peaks in the DOS, and the dominant peaks in MoTe$_2$ are marked by arrows in Fig. 5c, where the optical transitions correspond to the excitation energies of 2.52, 2.74, and 2.96 eV. In 2D materials, reduced electronic screening typically leads to strong excitonic effect. The Coulomb interaction of excited electrons and holes redistributes oscillator strength, giving rise to tightly bound excitons with eigenvalues lower than the band gap. By including electron-hole interactions, the optical transition energies between the DOS peaks are reduced to 2.22, 2.45, and 2.68 eV (shown in parentheses in Fig. 5c). With laser energies larger than 2.22 eV, the concentrations of excited carriers become higher, corresponding to strong optical excitation.

### Timescale of the phase transition

The timescale after laser excitation is divided into three regimes: (1) excited electrons thermalization (in 20 fs), (2) soft-mode phase transition (117–292 fs), and (3) lattice heating (within hundreds of ps).

**Table 1.** Excited carrier concentration $n$ and the maximum amount of excitation $N$.

| Energy (eV) | 1.58 | 1.96 | 2.34 | 2.42 | 2.63 |
|---|---|---|---|---|---|
| $n$ ($\times 10^{14}$ cm$^{-2}$) | 0.9 | 3.4 | 10.1 | 11.8 | 13.2 |
| $n/N_{tot}$ (%) | 0.8 | 2.9 | 8.5 | 9.9 | 11.1 |
| $N$ ($\times 10^{14}$ cm$^{-2}$) | 7.2 | 12.2 | 16.0 | 17.2 | 17.6 |
| $N/N_{tot}$ (%) | 6.0 | 10.2 | 13.5 | 14.5 | 14.8 |

Excited carrier concentration $n$ and the maximum amount of excitation $N$ by a laser pulse with a fluence of 100 mJ/cm$^2$, as well as their corresponding excitation percentage in the total number of valence electrons $N_{tot}$, at different laser excitation energies.

In the first stage, the temperature of the electronic system increases by photoexcitation and the excited electrons thermalize within 20 fs at a high electronic temperature, whereas the lattice remains cold. In photoexcited MoTe$_2$, carrier-carrier scattering is responsible for redistributing carrier energy, resulting in a thermalized distribution function of carriers[37]. The carrier relaxation time can be calculated from the quasiparticle self-energy[38,39]. The excited electrons thermalize in 20 fs (Fig. 5b), whereas the electron-hole recombination occurs on the order of picoseconds (see "Within 20 fs of Laser Excitation" in Supplementary Information). Thus, all the excited electrons are in thermal equilibrium before recombining or interacting with phonons.

In the second stage, the symmetry breaking displacements in 2H MoTe$_2$ take place within 292 fs. As the laser pulse creates electronic excitations, the new potential energy surfaces in Fig. 2a–c are formed immediately. The photo-induced lattice distortions, as a result of phonon softening, occur within the timescale of lattice vibrations. This can be estimated by the lattice vibration periods from 117 fs ($A_2''$ mode) to 292 fs ($E''$ mode). Such an estimate agrees well with previous molecular dynamics simulations[12] and pump-probe spectroscopy[24]. The structural distortion can take place before the electrons transfer their energy to the lattice by carrier-phonon interaction (1– 100 ps)[37].

In the third stage, the hot carriers are cooled by transferring energy to the lattice, converting electronic photoexcitation energy to heat in hundreds of picoseconds through interaction with various phonons.

### Competing mechanisms

One proposed mechanism for the PIPT in MoTe$_2$ is that after the excited electrons transfer their energy to the lattice through electron–phonon coupling, atomic reorganization toward the 1T' phase may occur as a result of local heat[20] or thermal strain[22,23]. We next demonstrate that these thermal effects alone cannot trigger the phase transition.

As the thermalized electronic system transfers its energy to the lattice, local heat is generated. The estimated local temperature during the laser irradiation is 670 K[9]. As the temperature increases, the phonons in the 1T' MoTe$_2$ phase are more highly excited than the phonons in the 2H MoTe$_2$ phase, because the 1T' phase has more low-energy phonons than the 2H phase (Fig. 6a). Thus, the entropy of the 1T' phase becomes higher than that of the 2H phase as temperature increases (the entropy increases with the occupancy). It is thereby possible for the 2H structure to transform into 1T' MoTe$_2$.

Thermodynamic stability at finite temperature can be described by the difference in Helmholtz free energy[40–42] (for the
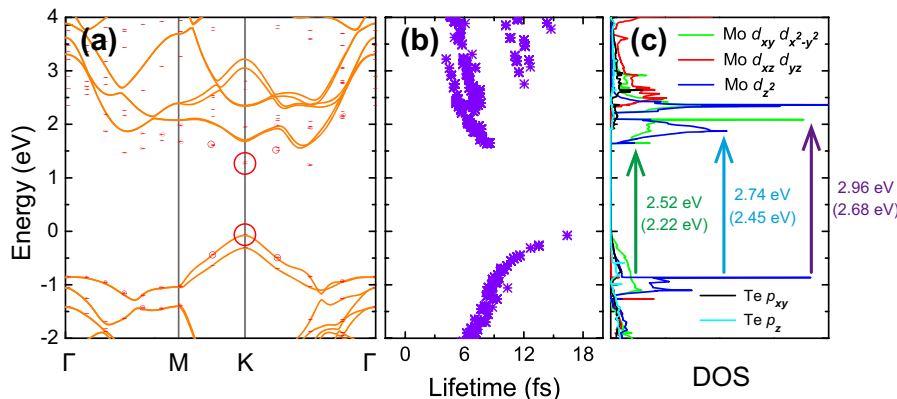


**Fig. 5 Electronic properties of 2H MoTe$_2$. a** Electronic structures, **b** quasiparticle relaxation time, and **c** DOS of monolayer MoTe$_2$. The red circles in **a** denote the first exciton. The radius of circles represents the electron-hole coupling coefficient of excitonic wave functions. The larger the radius, the more an electron-hole pair contributes to the exciton eigenstate. The arrows in **c** indicate optical transitions with different electronic excitation energies. The parentheses in **c** show the exciton excitation energies.
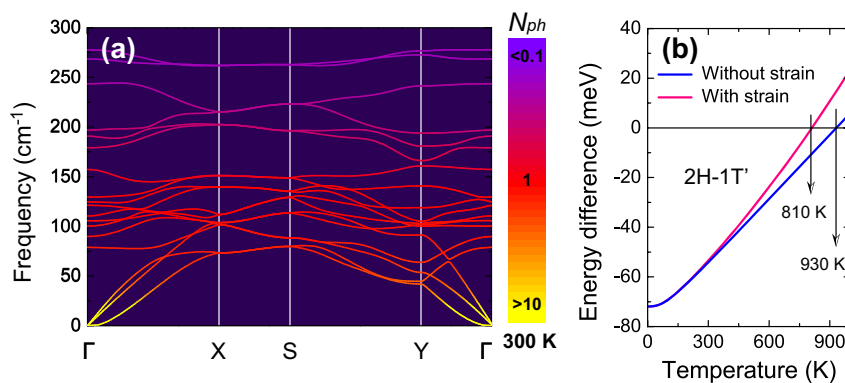
**Fig. 6 Thermodynamic stability of 2H and 1T′ MoTe₂ monolayers. a** Phonon dispersion of 1T′ MoTe₂ monolayer. The phonon occupation number is determined from the Bose–Einstein distribution function at 300 K. **b** Helmholtz free energy difference between 2H and 1T′ MoTe₂ monolayers as a function of temperature with and without thermal strain.

calculations of thermodynamic stability, see "Thermal Effects (about hundreds of ps)" in Supplementary Information). At 0 K, the free energy difference between the 2H phase and the 1T′ phase is just 72 meV per rectangular unit cell, indicating that the stability of the 1T′ phase is quite close to that of the 2H phase. As shown by the blue curve in Fig. 6b, at temperatures higher than 930 K, 1T′ MoTe₂ becomes thermodynamically more stable than 2H MoTe₂. This is consistent with the fact that the pure 1T′ phase appears in a temperature range between 930 K (for Te deficiency) and 1170 K (for Te excess)[43]. However, the temperature to facilitate the phase transition, 930 K, is significantly higher than the laser-induced temperature of 670 K[9]. Even after taking thermal strain into consideration [red curve in Fig. 6(b)], the phase transition temperature of 810 K is still higher than the laser-induced temperature (for the role of thermal strain, see "Thermal Effects (about hundreds of ps)" in Supplementary Information). Therefore, the laser-induced thermal effect on the phase transition has probably been overestimated in earlier studies[9,20].

In fact, previous experiments have suggested that the heating effect alone cannot induce the structural transformation[14]. For pure 2H MoTe₂, no significant change occurs after annealing, whereas laser irradiation leads to a mixed 2H + 1T′ phase. In the laser-irradiated mixed phase, the 2H phase disappears completely after annealing, leaving a pure 1T′ crystal[14]. Therefore, electronic excitation may drive spontaneous lattice distortions, whereas the heating effect accelerates the phase transition via thermal displacements, in which the intermediate states decay to the 1T′ phase (for the role of thermal displacement, see "Thermal Effects (about hundreds of ps)" in Supplementary Information).

Another proposed mechanism for the PIPT in MoTe₂ is that laser irradiation can create Te vacancies, which can trigger a local phase transition[9,20,21]. Consistent with this picture, a recent study has demonstrated that the phase transition involves a set of successive dynamics such as Te vacancy diffusion and ordering to generate the 1T′ phase[44], which is similar to the Ge-Sb-Te phase-change memory materials[45]. A vacancy-induced phase transition is related to a change in chemical composition, which is analogous to the composition-dependent phase transition in $Mo_{1-x}W_xTe_2$[46]. We emphasize that our work demonstrates that a phase transition can occur even in the absence of Te vacancies, and instead be driven by photoexcited carriers alone. Indeed, a recent experimental study has reported an electric-field induced structural transition in 2H MoTe₂[8], supporting our conclusion that changes in electron density alone can induce a phase transition without the need for Te vacancies. Similar photo-induced transitions have recently been predicted in the perovskites BaTiO₃ and PbTiO₃[47].

In summary, we demonstrate that a sub-picosecond phase transition in monolayer MoTe₂ from the 2H phase to a distorted 1T′ phase can be triggered by purely electronic excitation, even when the lattice is still cold. Such electronic excitation changes the electron density, resulting in a soft-mode displacive phase transition. The phase transition from the 2H phase to the 1T′ phase can be induced by a critical excitation energy of 1.96 eV, at which 2.9% of the carriers are excited. We also show that this phase transition mechanism can be understood in the frame of Landau theory and is quite different from a temperature-driven phase transition. The microscopic picture of the phase transition is analogous to a Peierls distortion, with a red shift of the conduction bands that are occupied upon photoexcitation that lowers the overall energy of the system. Our findings shed new light on the microscopic origin of PIPT in 2D transition-metal ditellurides and are expected to motivate both fundamental and applied studies of ultrafast phase transitions in these new class of materials for topological switching and neuromorphic computing.

## METHODS

All calculations are performed based on density functional theory (DFT) using the Vienna ab-initio simulation package[48]. The exchange-correlation energy is calculated within the generalized gradient approximation in the Perdew–Burke–Ernzerhof (PBE) parameterization[49]. In the excited state simulations, we mimic optical excitation by promoting valence electrons from high-lying valence band states to low-lying conduction band states. This method, typically called $\Delta$ self-consistent field[50–52], introduces noninteracting electron-hole pairs by changing the occupation numbers of the Kohn-Sham orbitals and is less computationally demanding than more advanced approaches such as constrained DFT[53] and excited-state force calculations within GW + BSE[54] but has been successfully used in studying PIPTs[12,55,56]. The occupied conduction band is determined by energy conservation at photoexcitation energies $E$ of 1.58 eV (785 nm), 1.96 eV (633 nm), 2.34 eV (532 nm), 2.42 eV (514 nm), and 2.63 eV (473 nm) (see "Computational Details" in Supplementary Information). We choose these laser excitation energies, because the corresponding wavelengths are experimentally feasible. We keep these occupancies fixed throughout the calculations. This scenario corresponds to the time domain of interest, namely, after the laser-excited carriers populate the states near the band edges but before these carriers relax to the band edges via electron–phonon interactions. Electron-hole recombination occurs on the picoseconds timescale, which is much larger than a single phonon period and therefore the number of excited electrons can be reasonably assumed to remain constant as in the calculation. It should be noted that, for simplicity, we use the PBE band structures to determine the number of the excited electrons under optical excitation. The GW₀ band structure correction is an almost rigid upshift of the PBE conduction bands of 0.69 eV, and after a simple scissor shift, the required laser excitation energies are still experimentally feasible. In subsequent work, it would be interesting to see how bound excitations (excitons) modify the picture.

## REFERENCES

1. Nasu, K. (ed) *Photo-Induced Phase Transitions* (World Scientific, 2004).
2. Bisoyi, H. K. & Li, Q. Light-driven liquid crystalline materials: from photo-induced phase transitions and property modulations to applications. *Chem. Rev.* **116**, 15089–15166 (2016).
3. Wu, J. M. & Liou, L. B. Room temperature photo-induced phase transitions of vo2 nanodevices. *J. Mater. Chem.* **21**, 5499–5504 (2011).
4. Koshihara, S., Tokura, Y., Mitani, T., Saito, G. & Koda, T. Photoinduced valence instability in the organic molecular compound tetrathiafulvalene-p-chloranil (ttf-ca). *Phys. Rev. B* **42**, 6853–6856 (1990).
5. Hanamura, E. In *Relaxations of Excited States and Photo-Induced Structural Phase Transitions* 34–44 (Springer-Verlag, Berlin, Heidelberg, 1997).
6. Wang, Y. et al. Structural phase transition in monolayer mote2 driven by electrostatic doping. *Nature* **550**, 487 (2017).
7. Fei, Z. et al. Ferroelectric switching of a two-dimensional metal. *Nature* **560**, 336–339 (2018).
8. Zhang, F. et al. Electric-field induced structural transition in vertical mote2- and mo1-xwxte2-based resistive memories. *Nat. Mater.* **18**, 55–61 (2019a).
9. Cho, S. et al. Phase patterning for ohmic homojunction contact in mote₂. *Science* **349**, 625 (2015).
10. Sie, E. J. et al. An ultrafast symmetry switch in a weyl semimetal. *Nature* **565**, 61–66 (2019).
11. Yang, H., Kim, S. W., Chhowalla, M. & Lee, Y. H. Structural and quantum-state phase transitions in van der waals layered materials. *Nat. Phys.* **13**, 931 (2017).
12. Kolobov, A. V., Fons, P. & Tominaga, J. Electronic excitation-induced semiconductor-to-metal transition in monolayer mote₂. *Phys. Rev. B* **94**, 094114 (2016).
13. Krishnamoorthy, A. et al. Semiconductor-metal structural phase transformation in mote2 monolayers by electronic excitation. *Nanoscale* **10**, 2742–2747 (2018).
14. Tan, Y. et al. Controllable 2h-to-1t' phase transition in few-layer mote2. *Nanoscale* **10**, 19964–19971 (2018).
15. Qian, X., Liu, J., Fu, L. & Li, J. Quantum spin hall effect in two-dimensional transition metal dichalcogenides. *Science* **346**, 1344 (2014).
16. Choe, D. H., Sung, H. J. & Chang, K. J. Understanding topological phase transition in monolayer transition metal dichalcogenides. *Phys. Rev. B* **93**, 125109 (2016).
17. Sajadi, E. et al. Gate-induced superconductivity in a monolayer topological insulator. *Science* **362**, 922 (2018).
18. Fatemi, V. et al. Electrically tunable low-density superconductivity in a monolayer topological insulator. *Science* **362**, 926 (2018).
19. Kretschmer, S., Komsa, H. P., Boggild, P. & Krasheninnikov, A. V. Structural transformations in two-dimensional transition-metal dichalcogenide mos2 under an electron beam: Insights from first-principles calculations. *J. Phys. Chem. Lett.* **8**, 3061–3067 (2017).
20. Wang, Z., Li, X., Zhang, G., Luo, Y. & Jiang, J. Suppressing electron-phonon coupling through laser-induced phase transition. *ACS Appl. Mater. Interfaces* **9**, 23309–23313 (2017).
21. Yoshimura, A., Lamparski, M., Kharche, N. & Meunier, V. First-principles simulation of local response in transition metal dichalcogenides under electron irradiation. *Nanoscale* **10**, 2388–2397 (2018).
22. Duerloo, K. A. N., Li, Y. & Reed, E. J. Structural phase transitions in two-dimensional mo- and w-dichalcogenide monolayers. *Nat. Commun.* **5**, 4214 (2014).
23. Song, S. et al. Room semiconductor-metal transition of mote2 thin films engineered by strain. *Nano Lett.* **16**, 188–193 (2016).
24. Zhang, M. Y. et al. Light-induced subpicosecond lattice symmetry switch in mote₂. *Phys. Rev. X* **9**, 021036 (2019b).
25. Kim, H. J., Kang, S. H., Hamada, I. & Son, Y. W. Origins of the structural phase transitions in mote₂ and wte₂. *Phys. Rev. B* **95**, 180101 (2017).
26. Yamamoto, M. et al. Strong enhancement of raman scattering from a bulk-inactive vibrational mode in few-layer mote2. *ACS Nano* **8**, 3895–3903 (2014).
27. Kan, M., Nam, H. G., Lee, Y. H. & Sun, Q. Phase stability and raman vibration of the molybdenum ditelluride (mote2) monolayer. *Phys. Chem. Chem. Phys.* **17**, 14866–14871 (2015).
28. Guo, H. et al. Double resonance raman modes in monolayer and few-layer mote₂. *Phys. Rev. B* **91**, 205415 (2015).
29. Dove, M.T. *Introduction to Lattice Dynamics* (Cambridge Univ. Press, 1993).
30. Dove, M. T. Review: theory of displacive phase transitions in minerals. *Am. Mineral.* **82**, 213 (1997).
31. Kittel, C. *Introduction to Solid State Physics* (Wiley, New York, 1976).
32. Zeks, B. & Blinc, R. *Soft Modes in Ferroelectrics and Antiferroelectrics* (North-Holland, 1974).
33. Monserrat, B. Electron-phonon coupling from finite differences. *J. Phys. Condens. Matter* **30**, 083001 (2018).
34. Song, Y. et al. Second harmonic generation in atomically thin mote2. *Adv. Opt. Mater.* **6**, 1701334 (2018).
35. Wall, S. et al. Ultrafast changes in lattice symmetry probed by coherent phonons. *Nat. Commun.* **3**, 721 (2012).
36. Bernardi, M., Vigil-Fowler, D., Lischner, J., Neaton, J. B. & Louie, S. G. Ab initio study of hot carriers in the first picosecond after sunlight absorption in silicon. *Phys. Rev. Lett.* **112**, 257402 (2014).
37. Shah, J. *Ultrafast Spectroscopy of Semiconductors and Semiconductor Nanostructures* (Springer Science & Business Media, 2013).
38. Kotani, T. & van Schilfgaarde, M. Impact ionization rates for si, gaas, inas, zns, and gan in the *gw* approximation. *Phys. Rev. B* **81**, 125201 (2010).
39. Peng, B. et al. Room-temperature bound exciton with long lifetime in monolayer gan. *ACS Photonics* **5**, 4081–4088 (2018a).
40. van Setten, M. J., Uijttewaal, M. A., de Wijs, G. A. & de Groot, R. A. Thermodynamic stability of boron: the role of defects and zero point motion. *J. Am. Chem. Soc.* **129**, 2458–2465 (2007).
41. Peng, B. et al. Stability and strength of atomically thin borophene from first principles calculations. *Mater. Res. Lett.* **5**, 399–407 (2017).
42. Peng, B. et al. Tuning thermal transport in c₃N monolayers by adding and removing carbon atoms. *Phys. Rev. Appl.* **10**, 034046 (2018b).
43. Keum, D. H. et al. Bandgap opening in few-layered monoclinic mote2. *Nat. Phys.* **11**, 482 (2015).
44. Si, C. et al. Photoinduced vacancy ordering and phase transition in mote2. *Nano Lett.* **19**, 3612–3617 (2019).
45. Zhang, W. et al. Role of vacancies in metal-insulator transitions of crystalline phase-change materials. *Nat. Mater.* **11**, 952–956 (2012).
46. Lv, Y. Y. et al. Composition and temperature-dependent phase transition in miscible mo1-xwxte2 single crystals. *Sci. Rep.* **7**, 44587 (2017).
47. Paillard, C., Torun, E., Wirtz, L., Íñiguez, J. & Bellaiche, L. Photoinduced phase transitions in ferroelectrics. *Phys. Rev. Lett.* **123**, 087601 (2019).
48. Kresse, G. & Furthmüller, J. J. Efficient iterative schemes for ab initio total-energy calculations using a plane-wave basis set. *Phys. Rev. B* **54**, 11169–11186 (1996).
49. Perdew, J. P., Burke, K. & Ernzerhof, M. Generalized gradient approximation made simple. *Phys. Rev. Lett.* **77**, 3865–3868 (1996).
50. Jones, R. O. & Gunnarsson, O. The density functional formalism, its applications and prospects. *Rev. Mod. Phys.* **61**, 689–746 (1989).
51. Görling, A. Density-functional theory for excited states. *Phys. Rev. A* **54**, 3912–3915 (1996).
52. Hellman, A., Razaznejad, B. & Lundqvist, B. I. Potential-energy surfaces for excited states in extended systems. *J. Chem. Phys.* **120**, 4593–4602 (2004).
53. Mauri, F. & Car, R. First-principles study of excitonic self-trapping in diamond. *Phys. Rev. Lett.* **75**, 3166–3169 (1995).
54. Ismail-Beigi, S. & Louie, S. G. Excited-state forces within a first-principles green's function formalism. *Phys. Rev. Lett.* **90**, 076401 (2003).
55. Li, X. B. et al. Role of electronic excitation in the amorphization of ge-sb-te alloys. *Phys. Rev. Lett.* **107**, 015501 (2011).
56. Chen, N. K. et al. Giant lattice expansion by quantum stress and universal atomic forces in semiconductors under instant ultrafast laser excitation. *Phys. Chem. Chem. Phys.* **19**, 24735–24741 (2017).

## AUTHOR CONTRIBUTIONS
H. Zhang, Z.-J.Q., and H. Zhu designed the research. B.P. and D.F. performed the calculations. D.F., B.P., H. Zhu, W.C., B.H., H.S., B.M., H.W., and C.M.S. analyzed and discussed the results. B.P., D.F., and H. Zhang wrote the text of the manuscript.

## COMPETING INTERESTS
The authors declare no competing interests.

## ADDITIONAL INFORMATION
**Supplementary information** is available for this paper at https://doi.org/10.1038/s41699-020-0147-x.

**Correspondence** and requests for materials should be addressed to H.Z., H.Z. or D.F.

**Reprints and permission information** is available at http://www.nature.com/reprints

**Publisher's note** Springer Nature remains neutral with regard to jurisdictional claims in published maps and institutional affiliations.